Eur. Phys. J. D (2022)76:242
https://doi.org/10.1140/epjd/s10053-022-00575-4

THE EUROPEAN PHYSICAL JOURNAL D

Regular Article – Atomic and Molecular Collisions

R-matrix calculation electron collisions with HCN and HNC molecules

Jasmeet Singh[1,2,a] and Jonathan Tennyson[2,b]

[1] Department of Physics, Keshav Mahavidyalaya, University of Delhi, Delhi 110034, India
[2] Department of Physics and Astronomy, University College London, Gower St, London WC1E 6BT, UK

Received 20 September 2022 / Accepted 30 November 2022

Abstract. Low energy electron collisions with hydrogen cyanide and hydrogen isocyanide molecules are studied using the R-matrix method. Scattering calculations are carried out using static exchange (SE), static exchange plus polarization (SEP) and close-coupling (CC) models. Electronic excitation cross sections are reported for HCN in our best 24-state close-coupling model with 17 virtual orbitals and for HNC using 25-state close-coupling model in which 18 virtual orbitals are included to account for polarization and correlation effects. These effects are necessary to obtain accurate results and also responsible for shift in the positions of $^2\Pi$ shape resonance (in both HCN and HNC) to lower energy compared to previous studies. These resonances are dissociative in nature. Complex resonance potential energy curves are produced for HCN and found to give narrower widths than previous theoretical results. Ionization cross section computed using Binary Encounter Bethe (BEB) method. Differential cross section (DCS) at 2, 4, 6, 8 and 10 eV and momentum transfer cross sections (MTCS) are also reported using 2-state CC model for HCN. The results obtained are useful for various research fields including plasma modelling and astrophysics.

1 Introduction

Hydrogen cyanide (HCN) is an important component of the atmospheres of exoplanets and is observable in emission from Comets [1–4]. Highly accurate spectroscopic data is required for the interpretation of astronomical spectra and to support astrophysics with upcoming instruments (telescopes) [5–9]. In star formation, electron excitation contributes to the emission from dense gas tracers in molecular clouds of high-dipole moment molecules [10] like HCN and HNC. The physical conditions in different parts of the interstellar medium can be interpreted in terms of the ratio of the isomers HCN and hydrogen isocyanide (HNC) [11].

The presence of a strong $^2\Pi$ shape resonance dominates the low-energy electron scattering from the HCN molecule and also leads to dissociative electron attachment via anion HCN^-. Such processes are important in the study of molecular plasma due their effect on the chemistry. Jain and Norcross [12] reported eigenphase sum and resonance potential energy curves as a function of the stretching C-H and C-N bonds. Chourou and Orel [13–15] published a series of complex Kohn variational calculations of resonance parameters as function of both the stretching and bending of the molecule obtaining a complex resonance potential energy surface. They reported dissociative electron attachment (DEA) cross section for these surfaces leading to CN^- and H computed using the multi-configuration time-dependent Hartree (MCTDH) approach. They found that it was necessary to accurately consider correlation and polarization effects [14] to reproduce the observed isotope effects in the system [16].

Sanz et al. [17] reported elastic, rotational and electronically inelastic (electronic excitation and ionization) cross section computed using the symmetry adapted-single centre expansion method for the energy range (0.1–100 eV) and optical potential method for intermediate and high energies (10–10000 eV). They compared elastic differential cross sections with the experimental results of [18] at 3, 5, 11.6, 21.6, 50 eV and with theoretical results of [19] at 3, 5, 11.6 eV.

Accurate data is required for plasma modelling and astrophysics; these data can be calculated by optimum use of available computational resources based on reliable theoretical methods. These theoretical methods not only provide a good description of the solution of the problem but also provide understanding of the processes involved.

Electron-impact excitation hyperfine-resolved rotational excitation cross sections and rates of HCN and HNC were calculated using the molecular R-matrix method combined with the adiabatic-nuclei-rotation approximation by Faure et al. [20]. Faure et al. also reported differential cross section at 5 eV.

[a] e-mail: jasmeet.singh@keshav.du.ac.in (corresponding author)
[b] e-mail: j.tennyson@ucl.ac.uk

Published online: 14 December 2022

In previous R-matrix study [21], the standard UK Molecular R-matrix code (UKRmol) [22] and Quantemol-N expert system [23] were used to compute the electron scattering cross sections for both HCN and HNC; this study included up to 4 target states in a close-coupling expansion (see Eq. (1)). The present calculations are performed using the Quantemol Electron Collisions (QEC) expert system [24]. QEC runs the UKRmol+ suites of codes [25] which are optimized to generate reliable scattering calculations, in part by using integration with the MOLPRO electronic structure package [26]. MOLPRO provides an accurate description of the molecular target including its symmetry. This combination, in the which R-matrix method is empowered by MOLPRO, gives a good description of scattering calculations for electron collisions with HCN and HNC molecules, using more complex target representations than the previous R-matrix study for the same number of excited states in the close-coupling expansion. Lower resonance positions and narrower resonance widths are found due to the better description of polarization and correlation effects which arises from use of an increased target basis set, inclusion of target states and virtual orbitals. No previous calculation mentioned the effect of inclusion of virtual orbitals on the scattering results of electron collision with HCN and HNC molecules. In comparison with the previous R-matrix calculations, a significant decrease in resonance position is found: about 0.5 eV for HCN and 0.4 eV for HNC. In this paper we focused on the low-energy elastic and excitation cross sections using the static exchange (SE), static exchange plus polarization (SEP) and close-coupling (CC) models along with potential energy curves, resonance parameters, ionization cross sections, differential cross section (DCS) and momentum transfer cross sections (MTCS).

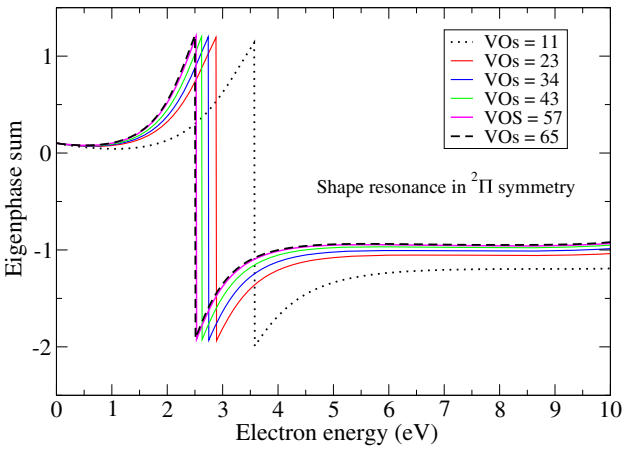

Fig. 1 Eigenphase sum in SEP model with different number of virtual orbitals for HCN

2 Calculations

2.1 R-matrix theory

The R-matrix method [27] is the most widely used *ab initio* method for studying electron-atom and electron-molecule collisions at low energies. Its implementation with the UK molecular R-matrix codes has been extensively discussed elsewhere [25,28], and we refer the reader to these works for details of the underlying theory.

The underlying assumption in the R-matrix method involves the division of configuration space into two regions: inner and outer which are separate by a sphere of radius a known as the R-matrix boundary. It assumed that the wave function of the N-electron target, $\phi_i^N(x_1 \dots x_N)$ below where i represents a state label, is entirely contained within the inner region. In this region the $(N+1)$-electron wave function can be written

$$\Psi_k^{N+1}(x_1 \dots x_{N+1}) = \mathcal{A} \sum_{ij} a_{ijk} \phi_i^N(x_1 \dots x_N) u_{ij}(x_{N+1}) + \sum_i b_{ik} \chi_i^{N+1}(x_1 \dots x_{N+1}) \quad (1)$$

where u_{ij} continuum orbital here represented by Gaussian type orbital (GTOs) [x]; $\mathcal{A}$ is the antisymmetrization operator which enforces the Pauli principle within the inner region. The second sum contains so-called L^2 configurations obtained by placing all electrons in target orbitals, including unoccupied (virtual) ones. The coefficients in Eq. (1) are obtained by diagonalizing a Hamiltonian matrix, constructed using an efficient purpose-built algorithm [x]. This step is energy independent and therefore only needs to be performed once per symmetry. The solutions of the inner region problem are used to construct the energy-dependent R-matrix at a which is then propagated to large distances to obtain the scattering observables, see Ref.[28] for further details.

2.2 Target calculations

The Quantemol Electron Collision (QEC) expert system [24], which runs both MOLPRO [26] and the new version of the UK molecular R-matrix code UKRMol+ [25], was used here to study the electron scattering from HCN and HNC molecules. QEC has been successfully used for low-energy collision cross-section calculations for a variety of molecular targets [29,30]. Here Gaussian type orbitals (GTOs) are used to represent both the target electrons and the scattering electron. Both HCN and HNC are linear closed shell molecules with $C_{\infty v}$ point group. Since MOLPRO, UKRMOL+ and QEC only allow Abelian point-groups, we use the C_{2v} point group to solve the scattering problem.

For these iso-electronic (HCN and HNC) molecules, the ground state electronic configuration is $1a_1^2$, $2a_1^2$, $3a_1^2$, $4a_1^2$, $5a_1^2$, $1b_1^2$ and $1b_2^2$. Of these 14 electrons,

Table 1 Vertical electronic excitation energy in eV, ground state energy in Hartree, the ground state dipole moment (μ) and polarizability (α) for HCN at its equilibrium geometry (C-H bond length 1.06 Å and C-N bond length 1.125 Å)

Target State $C_{\infty v}(C_{2v})$	Present results	[21]	Theory [31]	Experiment [32]
X $^1\Sigma^+(^1A_1)$	−93.024	−92.939 to −92.902		
1 $^3\Sigma^+(^3A_1)$	6.989	6.63 to 7.04	6.13	
1 $^3\Delta(^3A_1, ^3A_2)$	8.350	7.98 to 8.05	7.00	
1 $^3\Pi(^3B_1, ^3B_2)$	8.783	8.5 to 8.89	4.44	8.53 [33]
1 $^3\Sigma^-(^3A_2)$	9.067	8.67 to 8.97	5.47	
1 $^1\Sigma^-(^1A_2)$	9.517	8.98 to 9.23	6.48	6.48
1 $^1\Delta(^1A_1, ^1A_2)$	9.847	9.26 to 9.82	6.93	6.77
1 $^1\Pi(^1B_1, ^1B_2)$	10.158	9.83 to 10.18	8.10	8.10
2 $^3\Pi(^3B_1, ^3B_2)$	11.133	11.69 to 11.87	6.81	
2 $^1\Pi(^1B_1, ^1B_2)$	11.558	11.80 to 12.17	8.64	8.88
2 $^3\Sigma^+(^3A_1)$	11.683	12.16 to 12.61		
2 $^1\Sigma^+(^1A_1)$	11.862	12.24 to 12.76	7.79	
3 $^3\Sigma^+(^3A_1)$	15.151			
3 $^3\Pi(^3B_1, ^3B_2)$	16.011		7.47	
3 $^1\Sigma^+(^1A_1)$	16.037			
2 $^3\Delta(^3A_1, ^3A_2)$	16.304			
μ/D	2.61	2.87 to 3.07	3.03	2.98 [34]
α/Å^3	2.07		2.07 to 2.20 [34]	2.593 [34]

Table 2 Vertical electronic excitation energy in eV, ground state energy in Hartree, the ground state dipole moment (μ) and polarizability (α) for HNC at the equilibrium geometry (N-H bond length 0.982 Å and N-C bond length 1.146 Å)

Target State $C_{\infty v}(C_{2v})$	Present results	[21]	Theory [43]	Experiment
X $^1\Sigma^+(^1A_1)$	−93.009	−92.875 to −92.909		
1 $^3\Pi(^3B_1, ^3B_2)$	6.598	6.16 to 6.48		
1 $^3\Sigma^+(^3A_1)$	7.830	7.45 to 7.94	4.46	
1 $^3\Delta(^3A_1, ^3A_2)$	8.915	8.36 to 8.65	4.60	
1 $^1\Pi(^1B_1, ^1B_2)$	9.076	9.01 to 9.313	7.34	
1 $^3\Sigma^-(^3A_2)$	9.402	8.94 to 9.06	5.22	
1 $^1\Sigma^-(^1A_2)$	9.806	9.20 to 9.31	4.95	
1 $^1\Delta(^1A_1, ^1A_2)$	9.926	9.26 to 9.38	5.51	
2 $^3\Pi(^3B_1, ^3B_2)$	14.556	11.67 to 13.83		
2 $^1\Sigma^+(^1A_1)$	15.286	10.56 to 13.42	6.22	
3 $^3\Pi(^3B_1, ^3B_2)$	16.159			
2 $^1\Pi(^1B_1, ^1B_2)$	16.322	11.71 to 12.23	8.50	
4 $^3\Pi(^3B_1, ^3B_2)$	16.946			
3 $^1\Pi(^1B_1, ^1B_2)$	17.014			
5 $^3\Pi(^3B_1, ^3B_2)$	17.247			
μ/D	3.453	2.912 to 3.075		3.05 [34]
α/Å^3	2.17		2.255 to 2.369 [34]	

our complete active space configuration interaction (CASCI) target model froze four electrons in the $1a_1$, $2a_1$ orbitals and allowed ten electrons to move freely in nine active orbitals ($3a_1$, $4a_1$, $5a_1$, $6a_1$, $7a_1$, $1b_1$, $1b_2$, $2b_1$ and $2b_2$).

The MOLPRO program suite [26] was used to optimize the geometry of HCN and HNC. At equilibrium geometry of HCN, the CH bond length is 1.0565 Å and CN bond length is 1.1247 Å with ground state energy −93.024 Hartree using our CASCI model with a cc-pVTZ GTO basis. At the same level of the theory for HNC, the NH bond length is 0.9817 Å and NC bond length is 1.1456 Å with ground state energy −93.009 Hartree. These energies are lower than the previous R-matrix calculation [21] which used a smaller basis set and Hartree-Fock orbitals. .

Tables 1 and 2 present the vertical excitation energies of target states of HCN and HNC respectively for our best CASCI models. The position of excited states of HCN are close to previous theoretical studies [21]

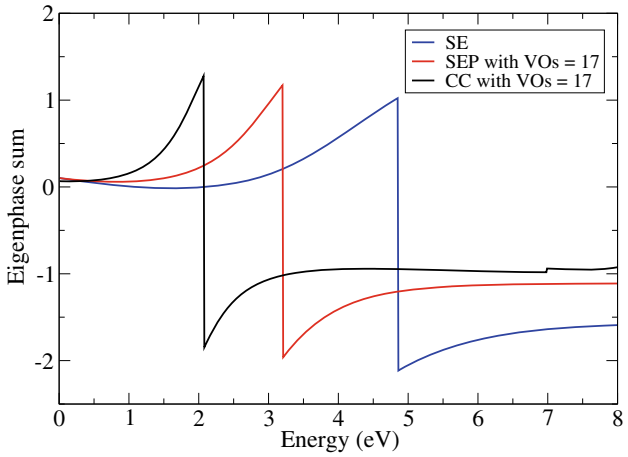

Fig. 2 Eigenphase sum in SE, SEP and CC models for HCN

Table 3 HCN $^2\Pi$ shape resonance parameters (in eV) for SE, SEP and CC models

Model	E_r	Γ_r
SE	4.310	2.932
SEP (with 65 VOs)	2.426	1.222
CC (with 17 VOs)	1.97	1.05
[21]	2.46 to 3.27	1.14 to 1.64
[19]	2.56 to 2.80	1.78 to 2.40
[36]	2.26	
[14]	1.905 to 4.353	1.17 to 5.986

Table 4 HNC $^2\Pi$ shape resonance parameters (in eV) for SE, SEP and CC models

Model	E_r	Γ_r
SE	4.418	2.444
SEP (with 50 VOs)	2.558	0.750
CC (with 18 VOs)	2.065	0.652
[21]	2.43 to 3.15	0.67 to 1.15

and [31], whereas the dipole moment is less than previous values reported in the same table. Results of HNC target states are compared with previous theoretical studies [21] and x in Table 2. The computed value of dipole moment for HNC is 3.453 D, which is higher than the previous studies using R-matrix method [21] and experimental value 3.05 D [34]. The polarizability values obtained using MOLPRO are in excellent agreement with [34]. Use of larger basis set, optimized geometry and inclusion of virtual orbitals in CC calculations made our results of vertical excitation energies different from previous calculations [21,31], x.

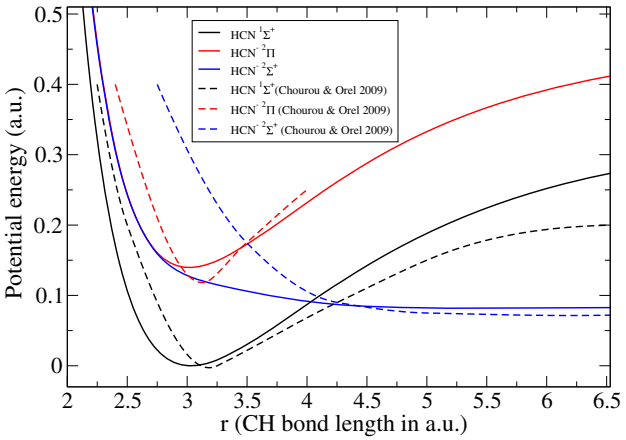

Fig. 3 Potential energy curves for HCN and HCN$^-$. Comparison of present results (using MOLPRO for HCN and QEC for the doublet HCN$^-$ states) with the work of Chourou and Orel [13]

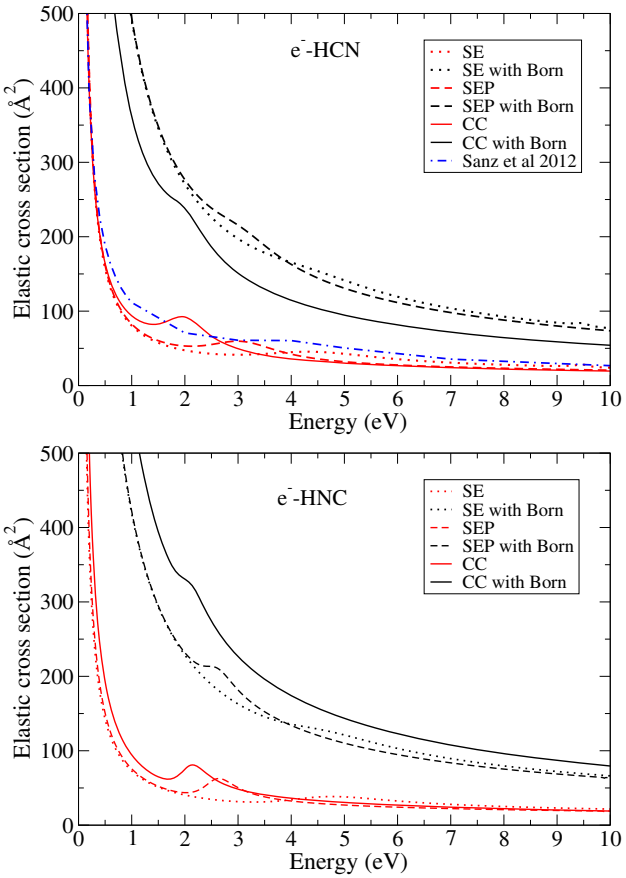

Fig. 4 Elastic cross sections from different models for electron collisions with HCN (upper panel) and HNC (lower panel). Red colour curves: without Born correction; black colour curves: with Born correction; dotted curves: SE; dashed curves: SEP; solid curves: CC

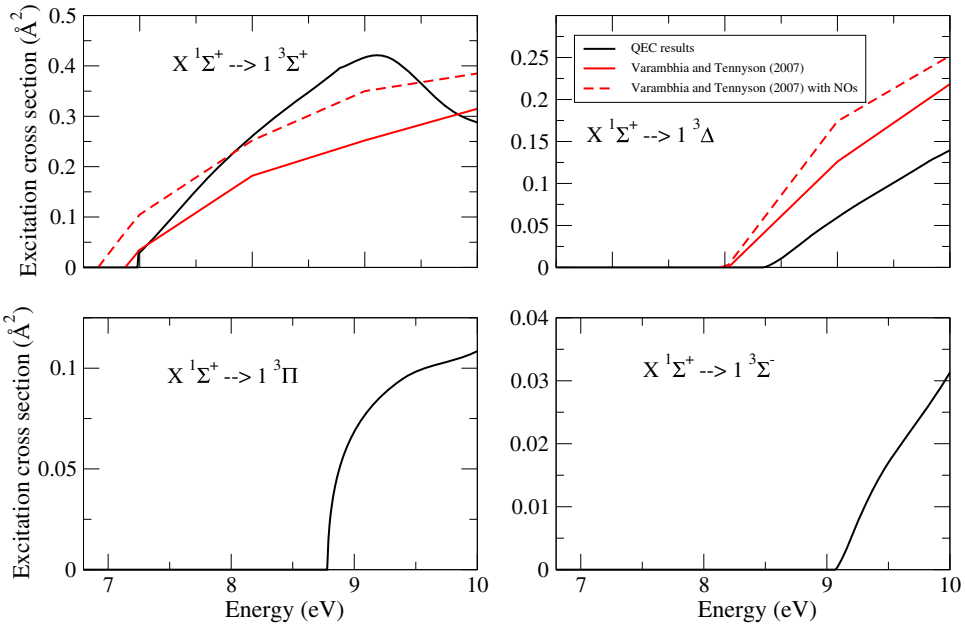

Fig. 5 Electronic excitation cross section for electron collisions with HCN. Comparison of R-matrix calculations (using QEC) with previous study by Varambhia and Tennyson [21]

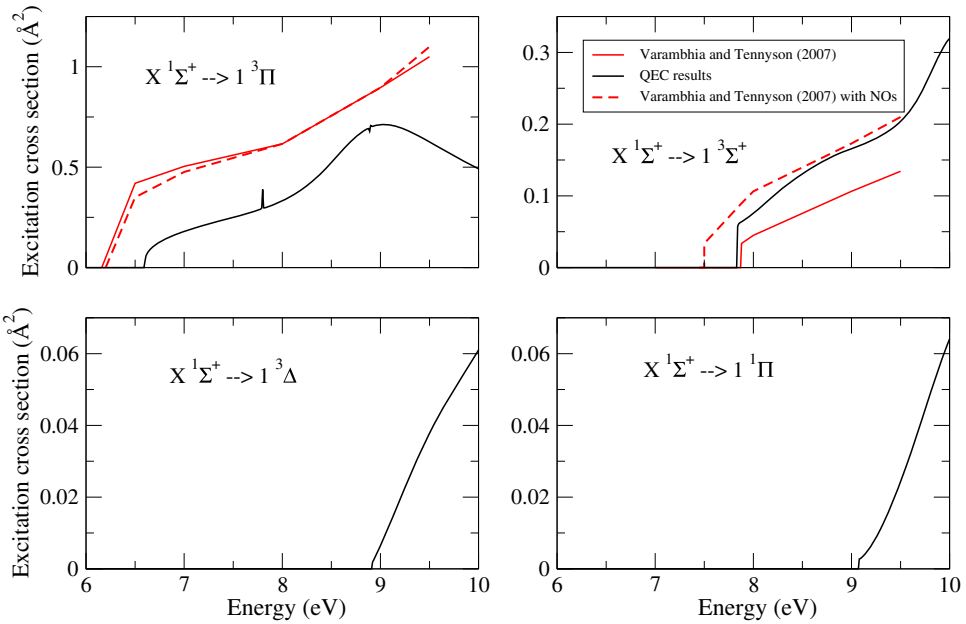

Fig. 6 Electronic excitation cross section for electron collisions with HNC. Comparison of R-matrix calculations (using QEC) with previous study by Varambhia and Tennyson [21]

2.3 Scattering calculations

We started the calculations with the SE model in which all target electrons are frozen. In this model, the incoming scattering electron is not allowed to polarize the Hartree-Fock target wave function. Shape resonance are detected in the SE model, albeit at higher energies, but Feshbach or core-excited resonances cannot be detected. For a better description of the scattering, extra L^2 configurations are added in the SEP model which allow for polarization effects. In SEP model, one electron from the Hartree-Fock target wave function is promoted to a virtual orbital and also the scattering electron placed in a target virtual orbital. We performed SEP calculations by including increasing numbers of virtual orbitals (shown in Fig. 1) to achieve more accurate resonance parameters and cross-sections; our best model is the CC model for which the shape resonance lies at lower energy than SE and any SEP run, see Fig. 2. In the CC expansion, target electronic states are

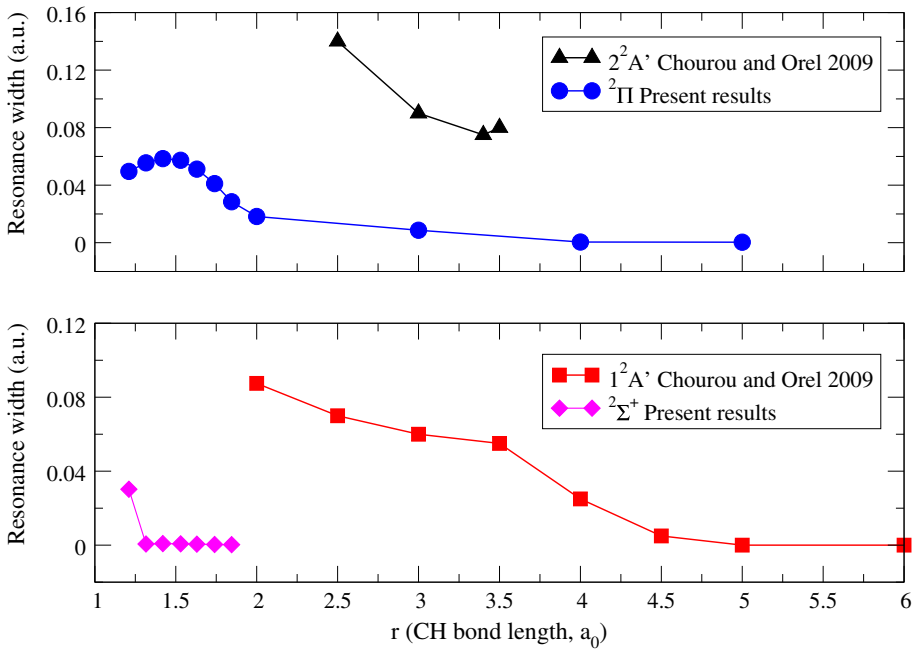

Fig. 7 Resonance widths for HCN. Comparison of present results those of with Chourou and Orel [13]

included which are described using a complete active space (CAS) [35]. In this model some target electrons are frozen while some are free to move in active space which produces more correlation effects. This journey to arrive at our best model (for both HCN and HNC) was very challenging as theoretical calculations depend on various factors like geometry, basis set, active space and choice of target wave functions to get reliable results for outer region calculations by optimum use of present computing resources. Our final model used a 24-target states CC-model (including 17 virtual orbitals) for HCN and a 25-target states CC-model (including 18 virtual orbitals) for HNC, both used cc-pVTZ GTO basis set to represent the target.

2.3.1 Electron scattering from HCN

For the CC calculations, seventeen HCN virtual orbitals are included in our final scattering calculations, seven of A_1 symmetry ($8a_1$, $9a_1$, $10a_1$, $11a_1$, $12a_1$, $13a_1$, $14a_1$), four of B_1 symmetry ($3b_1$, $4b_1$, $5b_1$, $6b_1$), four of B_2 symmetry ($3b_2$, $4b_2$, $5b_2$, $6b_2$) and two of A_2 symmetry ($1a_2$, $2a_2$). The electron cloud of all target electrons of HCN is enclosed in a radius of 10 a_0 of inner region. 24 target states were included in the HCN CC run, which is the same as the previous R-matrix calculation [21] which, however, used a smaller basis set. 24-state CC trial runs with different number of virtual orbitals (VOs) were performed. Trials with more than 17 VOs were unsuccessful as they exceeded the available computer memory. So we arrived at a maximum number of 17 VOs to be included in the CC run. However, all the VOs (= 65) can be included in the SEP run but our best 24-state CC-model uses 17 VOs; note that this is equivalent to a 24 VO SEP model as 7 VOs are in the target CAS. This CC model gives the position of $^2\Pi$ shape resonance 0.5 eV lower than the SEP model even with all VOs (in Table 3). This is due to the inclusion of excited states in the CC model which, in particular, give a representation of polarization in the outer region (via the dipole coupling to excited states) which is absent in the SEP model.

2.3.2 Electron scattering from HNC

Similar CC calculations were performed for HNC. Fifty virtual orbitals (VOs = 50) were included in our SEP model but our best model is the 25 state CC-model with eighteen virtual orbitals (8 to 15 a_1, 3 to 6 b_1, 3 to 6 b_2 and 1 to 2 a_2). By increasing the number of virtual orbitals in the CC calculations, the position of $^2\Pi$ shape resonance 0.5 eV is lower than the SEP model with 50 VOs (in Table 4).

3 Results and discussions

3.1 Potential energy curves

Potential energy curves for ground state of HCN ($^1\Sigma^+$) and HCN^- ($^2\Pi$ and $^2\Sigma^+$) were produced directly from MOLPRO program using our CAS with a cc-pVTZ basis set for various geometries of the molecule by stretching the C-H bond of HCN molecule in the range from 0.4565 to 3.4565 Å with a grid 0.01 Å. Figure 3 compares the potential energy curves with the results of Chourou and Orel [13] who used a multi-reference configuration interaction (MRCI) method. Our PECs are

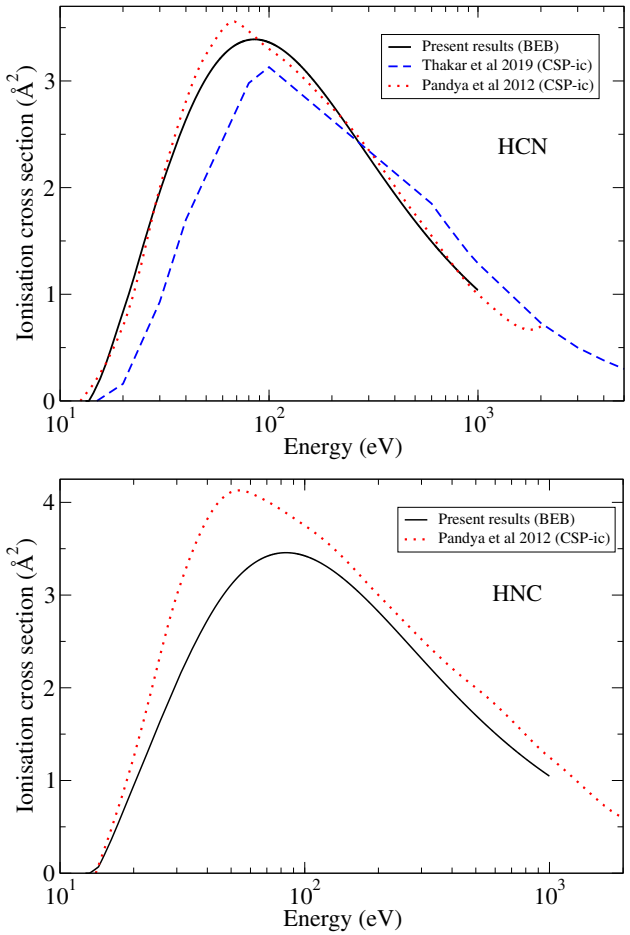

Fig. 8 Electron ionization cross section of HCN (upper panel) and HNC (lower panel) molecules; solid-present results from BEB, dot-CSP-ic results of [40], dash-CSP-ic results of [41]

in good shape in comparison with the curves of [13]. The crossing of our curves for $^1\Sigma^+$ and $^2\Sigma^+$ state at 4 a_0 C-H bond length is higher than crossing point 2.8 a.u. of Jain and Norcross [12] but lower than [13] which occur at 4.25 a_0.

3.2 Elastic and inelastic cross sections

The elastic cross sections for HCN and HNC for SE, SEP and CC models are presented in Fig. 4. The results for HCN are in good agreement with [17]. The presence of $^2\Pi$ shape resonance can be seen in all three types of cross sections for both molecules. The position of the resonance shifts to lower energy on inclusion of polarization and correlation effects. In Figs. 5 and 6, excitation cross section of first four transition to excited states ($^3\Sigma^+$, $^3\Delta$, $^3\Pi$ and $^3\Sigma^-$) of HCN and ($^3\Pi$, $^3\Sigma^+$, $^3\Delta$ and $^1\Pi$) of HNC is shown, respectively. A comparison with the previous R-matrix calculation by Varambhia and Tennyson [21] is shown in these figures. They reported cross sections with and without natural orbitals (NOs). The cross sections of [21] are higher suggesting that increasing the basis set leads to a significant reduction in the electronic excitation cross sections.

3.3 Resonance properties

A Breit-Wigner profile fit to the eigenphase sums was used to characterize resonances, and hence, resonance positions and widths were obtained using the program RESON [37]. The resonance parameters of $^2\Pi$ shape resonance in different models are presented and compared with the previous results [14,19,21,36] in Table 3 for electron collision with HCN. In Table 4, a similar comparison is reported and compared with [21] for HNC. Our results for HCN (lower resonance position at 1.97 eV and narrow resonance width about 1.05 eV) are better than the previous reported resonance parameters due to use of better basis set, inclusion of more polarization and correlation effects. No previous work on HCN and HNC molecules mentioned the effect of inclusion of different number of virtual orbitals in the scattering calculations, although such studies have been performed on other systems [38]. In comparison with the previous R-matrix calculations [21], the decrease in resonance position for both is significant, 0.5 eV for HCN and 0.4 eV for HNC.

Figure 7 compares the resonance widths for HCN; ours are found to be narrower than those of Chourou and Orel [13]. In the later studies, Chourou and Orel [14,15] imply that improving the treatment of polarization in their scattering calculation (which presumably lowers the resonance energies and narrows the widths) gave better agreement with experiment. Note that the $^2\Pi$ widths go to zero at large bond length (C-H bond length, r = 4 Bohr) as the resonance becomes bound en route to dissociation.

3.4 Ionization cross section

In QEC, the ionization cross section (ICS) is computed by using the binary-encounter Bethe (BEB) method [39]. According to BEB, the cross section σ_{BEB} is given by,

$$\sigma_{\mathrm{BEB}} = \frac{S}{t+u+1}\left[\frac{1}{2}\left(1-\frac{1}{t^2}\right)\ln t + 1 - \frac{1}{t} - \frac{\ln t}{1+t}\right], \tag{2}$$

where $t = T/B, u = U/B$, and $S = 4\pi a_0^2 N(R/B)^2$. a_0 is the Bohr radius, and R is the Rydberg energy. B, U, and N are the binding energy, the kinetic energy, and the occupation number, respectively, for the subshell. If the kinetic energy T of the incident electron is less than B, then $\sigma_{BEB} = 0$.

In Fig. 8, the maximum of ICS for HCN at 85.2 eV with a value of 3.4 Å^2 using BEB. The present peak value is in fair agreement with the results 3.55 Å^2 at 70 eV using complex potential ionization contribution (CSP-ic) method [40]. Another recent study [41] on electron interactions with astro chemical compounds

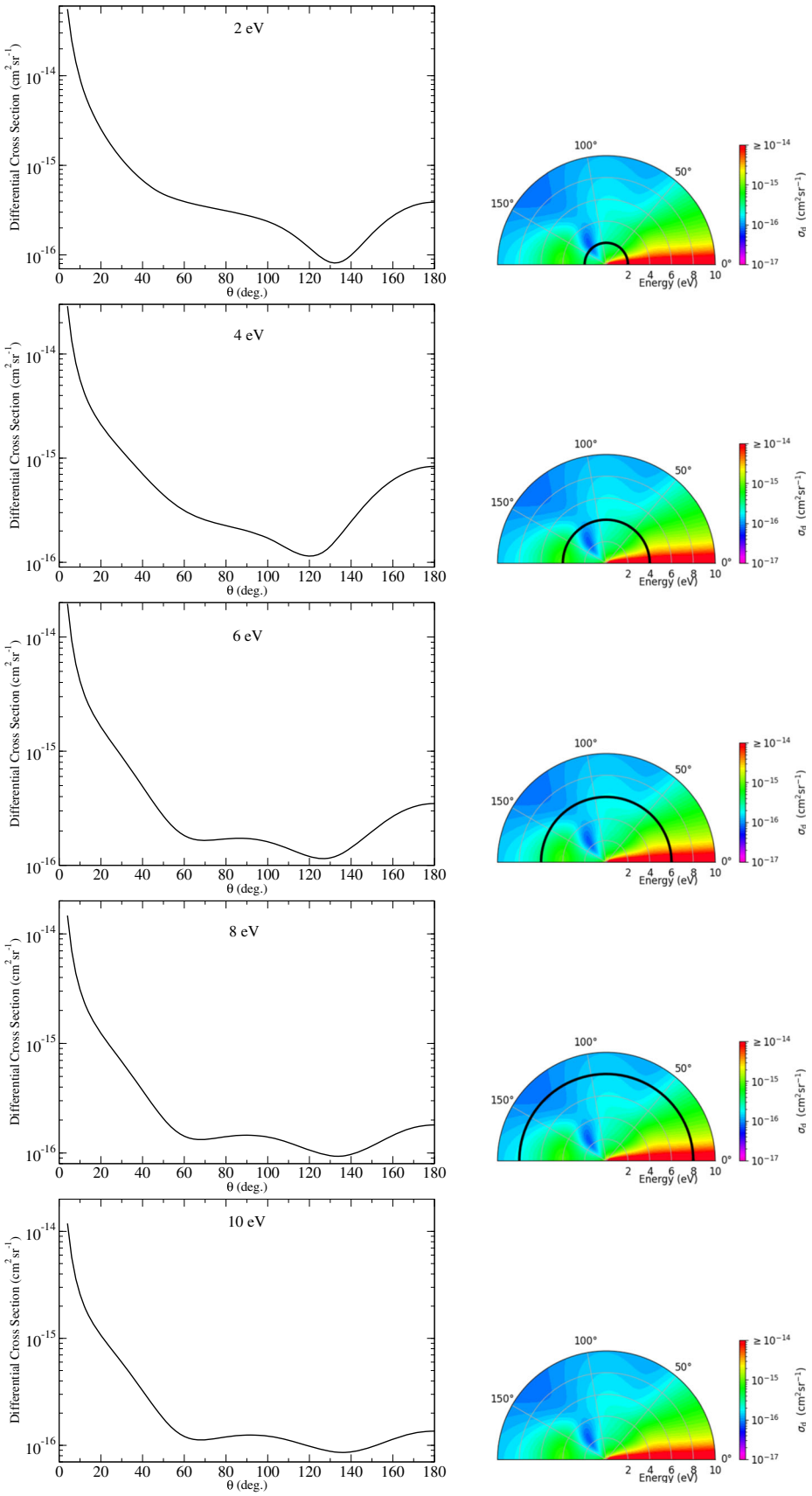

Fig. 9 Differential cross section at 2, 4, 6, 8 and 10 eV for HCN

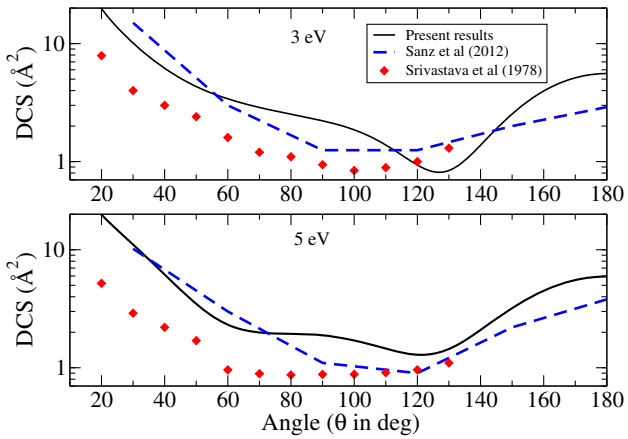

Fig. 10 Comparison of differential cross section with previous theoretical results [17] and experimental results [18] at 3 and 5 eV for HCN

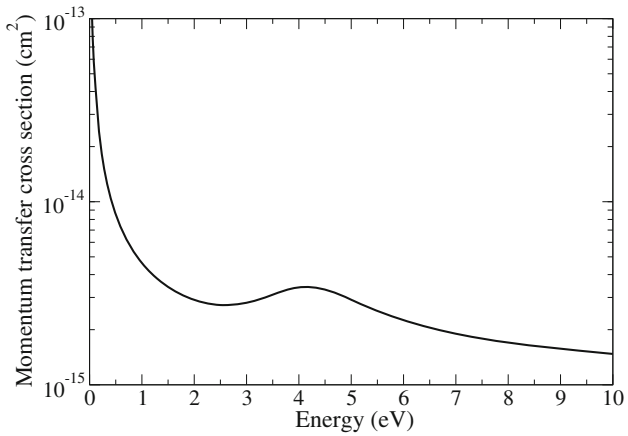

Fig. 11 Momentum transfer cross section for HCN

used the same formalism (CSP-ic) and reported ionization cross section maximum value 3.13 Å^2 of the curve at 100 eV, with accuracy of $\pm 10-20$ %.

For HNC the maximum occur at 84.45 eV with a value of 3.45 Å^2 using BEB. Pandya et al. [40] used CSP-ic method to compute ICS with a peak value 4.1 Å^2 at 60 eV. As extensive comparisons of BEB with experiments suggest that BEB cross sections are generally reliable but have a slight tendency to underestimate the peak [42], we would suggest that Pandya et al.'s ionization cross section for HNC is too high.

3.5 Differential cross section

In Fig. 9 the DCS for HCN is shown for different energies 2, 4, 6, 8 and 10 eV. At forward scattering angles, the DCS has maximum value and then gradually decreases as the angle of scattering is increased. The DCS shows a minima in between 120° to 140° for all energy values. Figure 10 shows a comparison with previous theoretical results [17] and experimental results [18] at electron energy 3 and 5 eV.

3.6 Momentum transfer cross section

In Fig. 11, momentum transfer cross sections for HCN are shown. A bump is observed around 4.15 eV which corresponds to the shape resonance.

4 Conclusion

With QEC, this challenging task of performing R-matrix calculations with larger basis sets using the SE, SEP and with 24 target state CC models for HCN and 25 target state CC models for HNC for electron scattering energies up to 10 eV completed. The effect of using different numbers of virtual orbitals in the calculation to represent short-range polarization effects is tested. Due to more polarization and correlation effects which increases with use of large basis set, inclusion of target states and more virtual orbitals, our results are better than previous R-matrix calculations, specifically lower resonance positions and narrow resonance widths. We believe this accurate results obtained are useful for various research fields including plasma modelling and astrophysics, as well as providing support for experimental studies.

Acknowledgements We thank Su He for help setting up the calculations. This work was supported by 'The Royal Society London, UK' under International Exchange Scheme (ref: IES\ R3 \193159 International Exchanges 2019 Round 3).

Declarations

Data Availability Statement This manuscript has no associated data or the data will not be deposited. [Authors' comment:. The data generated in this work are given in the paper. Numerical values for data given graphically will be provided upon reasonable requests to the authors.

Author Contribution Statement JS performed the calculations and made the original draft of the manuscript; JT advised on the calculations and edited the manuscript.

References

1. P.B. Rimmer, S. Rugheimer, Hydrogen cyanide in nitrogen-rich atmospheres of rocky exoplanets. Icarus **329**, 124–131 (2019)
2. P. Rimmer, M. Ferus, I. Waldmann, A. Knížek, D. Kalvaitis, O. Ivanek, P. Kubelík, S. Yurchenko, T. Burian, J. Dostál et al., Identifiable acetylene features predicted for young earth-like exoplanets with reducing atmospheres undergoing heavy bombardment. Astrophys J **888**(1), 21 (2019)
3. M.R. Swain, R. Estrela, G.M. Roudier, C. Sotin, P.B. Rimmer, A. Valio, R. West, K. Pearson, N. Huber-Feely, R.T. Zellem, Detection of an atmosphere on a rocky exoplanet. Astron. J. **161**(5), 213 (2021)

4. P. Bergman, M. Lerner, A. Olofsson, E. Wirström, J.H. Black, P. Bjerkeli, R. Parra, K. Torstensson, Emission from hcn and ch3oh in comets-onsala 20-m observations and radiative transfer modelling. Astronom. Astrophys. **660**, 118 (2022)
5. RP.R. Roelfsema, H. Shibai, L. Armus, D. Arrazola, M. Audard, M.D. Audley, C.M. Bradford, I. Charles, P. Dieleman, Y. Doi, L. Duband, M. Eggens, J. Evers, I. Funaki, J.R. Gao, M. Giard, A. di Giorgio L.M. González Fernández, M. Griffin, F.P. Helmich, R. Hijmering, R. Huisman, D. Ishihara, N. Isobe, B. Jackson, H. Jacobs, W. Jellema, I. Kamp, H. Kaneda, M. Kawada, F. Kemper, F. Kerschbaum, P. Khosropanah, K. Kohno, P.P. Kooijman, O. Krause, J. van der Kuur, J. Kwon, W.M. Laauwen, G. de Lange, B. Larsson, D. van Loon, S.C. Madden, H. Matsuhara, F. Najarro, T. Nakagawa, D. Naylor, H. Ogawa, T. Onaka, S. Oyabu, A. Poglitsch, V. Reveret, L. Rodriguez, L. Spinoglio, I. Sakon, Y. Sato, K. Shinozaki, R. Shipman, H. Sugita, T. Suzuki, F.F.S. van der Tak, J. Torres Redondo, T. Wada, S.Y. Wang, C.K. Wafelbakker, H. van Weers, S. Withington, B. Vandenbussche, T. Yamada, I. Yamamura, SPICA–a large cryogenic infrared space telescope: unveiling the obscured universe. Publ. Astron. Soc. Aust. (2018) https://doi.org/10.48550/arXiv.1803.10438
6. B.R. Brandl, Bernhard R, O, Absil, T. Agócs, N. Baccichet, T. Bertram, F. Bettonvil, R. van Boekel, L. Burtscher, E. van Dishoeck, M. Feldt, et al., Status of the mid-IR ELT imager and spectrograph (METIS). Ground-based and Airborne Instrumentation for Astronomy VII. vol. 10702, pp. 582–596 (2018)
7. G. S. Wright, David Wright, G. B. Goodson, G. H. Rieke, Gabby Aitink-Kroes, J. Amiaux, Ana Aricha-Yanguas, Ruymán Azzollini, Kimberly Banks, D. Barrado-Navascues, T. Belenguer-Davila, J. A. D. L. Bloemmart, Patrice Bouchet, B. R. Brandl, L. Colina, Örs Detre, Eva Diaz-Catala, Paul Eccleston, Scott D. Friedman, Macarena García-Marín, Manuel Güdel, Alistair Glasse, Adrian M. Glauser, T. P. Greene, Uli Groezinger, Tim Grundy, Peter Hastings, Th. Henning, Ralph Hofferbert, Faye Hunter, N. C. Jessen, K. Justtanont, Avinash R. Karnik, Mori A. Khorrami, Oliver Krause, Alvaro Labiano, P.-O. Lagage, Ulrich Langer, Dietrich Lemke, Tanya Lim, Jose Lorenzo-Alvarez, Emmanuel Mazy, Norman McGowan, M. E. Meixner, Nigel Morris, Jane E. Morrison, Friedrich Müller, H.-U. Nø rgaard-Nielson, Göran Olofsson, Brian O'Sullivan, J.-W. Pel, Konstantin Penanen, M. B. Petach, J. P. Pye, T. P. Ray, Etienne Renotte, Ian Renouf, M. E. Ressler, Piyal Samara-Ratna, Silvia Scheithauer, Analyn Schneider, Bryan Shaughnessy, Tim Stevenson, Kalyani Sukhatme, Bruce Swinyard, Jon Sykes, John Thatcher, Tuomo Tikkanen, E. F. van Dishoeck, C. Waelkens, Helen Walker, Martyn Wells, and Alex Zhender, The mid-infrared instrument for the james web space telescope, ii: Design and build. Publ. Astron. Soc. Pacific. **127**(953), 595 (2015)
8. F.F. van der Tak, F. Lique, A. Faure, J.H. Black, E.F. van Dishoeck, The leiden atomic and molecular database (lamda): current status, recent updates, and future plans. Atoms **8**(2), 15 (2020)
9. R.J. Barber, J.K. Strange, C. Hill, O.L. Polyansky, G.C. Mellau, S.N. Yurchenko, J. Tennyson, ExoMol line lists - III. An improved hot rotation-vibration line list for HCN and HNC. Mon. Not. R. Astron. Soc. **437**, 1828–1835 (2014). https://doi.org/10.1093/mnras/stt2011
10. P.F. Goldsmith, J. Kauffmann, Electron excitation of high dipole moment molecules re-examined. Astrophys J **841**(1), 25 (2017)
11. A. Zamir, T. Stein, Isomerization of hydrogen cyanide and hydrogen isocyanide in a cluster environment: quantum chemical study. J. Chem. Phys. **156**(5), 054307 (2022)
12. A. Jain, D. Norcross, Ab initio calculations of low-energy electron scattering by HNC molecules: dependence on internuclear distance in linear geometry. J. Chem. Phys. **84**(2), 739–744 (1986)
13. S. Chourou, A. Orel, Dissociative electron attachment to HNC and HNC. Phys. Rev. A **80**(3), 032709 (2009)
14. S. Chourou, A. Orel, Isotope effect in dissociative electron attachment to HNC. Phys. Rev. A **83**(3), 032709 (2011)
15. S. Chourou, A. Orel, Dissociative electron attachment to HNC, HCCH and HCCCH. J. Phys: Conf. Ser. **300**(1), 012014 (2011). (**IOP Publishing**)
16. O. May, D. Kubala, M. Allan, Absolute cross sections for dissociative electron attachment to HCN and DCN. Phys. Rev. A **82**(1), 010701 (2010)
17. A. Sanz, M. Fuss, F. Blanco, F. Sebastianelli, F. Gianturco, G. García, Electron scattering cross sections from hcn over a broad energy range (0.1–10 000 ev): Influence of the permanent dipole moment on the scattering process. J. Chem. Phys. **137**(12), 124103 (2012)
18. S. Srivastava, H. Tanaka, A. Chutjian, Elastic scattering of intermediate energy electrons by hcn. J. Chem. Phys. **69**(4), 1493–1497 (1978)
19. A. Jain, D. Norcross, Ab initio calculations of low-energy electron scattering by HCN molecules. Phys. Rev. A **32**(1), 134 (1985)
20. A. Faure, H.N. Varambhia, T. Stoecklin, J. Tennyson, Electron-impact rotational and hyperfine excitation of HCN, HNC, DCN and DNC. Mon. Not. R. Astron. Soc. **382**(2), 840–848 (2007)
21. H.N. Varambhia, J. Tennyson, Electron collision with the HCN and HNC molecules using the r-matrix method. J. Phys. B: At. Mol. Opt. Phys. **40**(6), 1211 (2007)
22. J.M. Carr, P.G. Galiatsatos, J.D. Gorfinkiel, A.G. Harvey, M.A. Lysaght, D. Madden, Z. Mašín, M. Plummer, J. Tennyson, H.N. Varambhia, The ukrmol program suite. Eur. Phys. J. D **66**, 58 (2012)
23. J. Tennyson, D.B. Brown, J.J. Munro, I. Rozum, H.N. Varambhia, N. Vinci, Quantemol-N: an expert system for performing electron molecule collision calculations using the R-matrix method. J. Phys: Conf. Ser. **86**, 012001 (2007)
24. B. Cooper, M. Tudorovskaya, S. Mohr, A. O'Hare, M. Hanicinec, A. Dzarasova, J.D. Gorfinkiel, J. Benda, Z. Mašín, A.F. Al-Refaie et al., Quantemol electron collisions (qec): an enhanced expert system for performing electron molecule collision calculations using the r-matrix method. Atoms **7**(4), 97 (2019)

25. Z. Mašín, J. Benda, J.D. Gorfinkiel, A.G. Harvey, J. Tennyson, Ukrmol+: A suite for modelling electronic processes in molecules interacting with electrons, positrons and photons using the r-matrix method. Comput. Phys. Commun. **249**, 107092 (2020)
26. H.-J. Werner, P.J. Knowles, R. Lindh, F.R. Manby, M. Schütz, P. Celani, W. Györffy, D. Kats, T. Korona, R. Lindh et al. Molpro, a package of ab initio programs. http://www.molpro.net Version 2009.1
27. P.G. Burke, R-matrix theory of atomic collisions: Application to atomic, molecular and optical processes (2011)
28. J. Tennyson, Electron-molecule collision calculations using the r-matrix method. Phys. Rep. **491**(2–3), 29–76 (2010)
29. D. Gupta, H. Choi, D.-C. Kwon, H. Su, M.-Y. Song, J.-S. Yoon, J. Tennyson, Low-energy electron scattering from c-c4f8. Atoms **10**(2), 63 (2022)
30. H. Su, X. Cheng, B. Cooper, J. Tennyson, H. Zhang, Electron-impact high-lying n 2- resonant states. Phys. Rev. A **105**(6), 062824 (2022)
31. M.K. Nayak, R.K. Chaudhuri, S. Krishnamachari, Theoretical study on the excited states of hcn. J. Chem. Phys. **122**(18), 184323 (2005)
32. G. Herzberg, Electronic spectra and electronic structure of polyatomic molecules **vol. 3** (1966)
33. S. Krishnamachari, R. Venkatasubramanian, Electronic absorption spectra of hnc and dnc. Spectrosc. Lett. **19**(1), 55–60 (1986)
34. Nist: Triatomic spectral database. https://physics.nist.gov/cgi-bin/MolSpec/triperiodic.pl
35. J. Tennyson, R-matrix calculation of Rydberg states of CO. J. Phys. B: At. Mol. Opt. Phys. **29**, 6185–6201 (1996)
36. P. Burrow, A. Howard, A. Johnston, K. Jordan, Temporary anion states of hydrogen cyanide, methyl cyanide, and methylene dicyanide, selected cyanoethylenes, benzonitrile, and tetracyanoquinodimethane. J. Phys. Chem. **96**(19), 7570–7578 (1992)
37. J. Tennyson, C.J. Noble, Reson-a program for the detection and fitting of breit-wigner resonances. Comput. Phys. Commun. **33**(4), 421–424 (1984)
38. M.M. Fujimoto, W.J. Brigg, J. Tennyson, R-matrix calculations of differential and integral cross sections for low-energy electron collisions with ethanol. Eur. Phys. J. D **66**, 204 (2012)
39. Y.K. Kim, M.E. Rudd, Binary-encounter-dipole model for electron impact ionisation. Phys. Rev. A **50**, 3954 (1994)
40. S.H. Pandya, F.A. Shelat, K. Joshipura, B.G. Vaishnav, Electron ionization of exotic molecular targets cn, c2n2, hcn, hnc and bf-theoretical cross sections. Int. J. Mass Spectrom. **323**, 28–33 (2012)
41. Y. Thakar, R. Bhavsar, M. Swadia, M. Vinodkumar, N. Mason, C. Limbachiya, Electron interactions with astro chemical compounds. Planet. Space Sci. **168**, 95–103 (2019)
42. V. Graves, B. Cooper, J. Tennyson, The efficient calculation of electron impact ionization cross sections with effective core potential. J. Chem. Phys. 154, 114104. DOI https://doi.org/10.1063/5.0039465 (2021)
43. G.M. Schwenzer, H.F. Schaefer III, C.F. Bender, Excited electronic states of HNC, hydrogen isocyanide. J. Chem. Phys. **63**(1):569–572